Electronic Supplementary Information (ESI)

Metal nanoparticle assembly with broadband absorption and suppressed thermal radiation for enhanced solar steam generation

Dawei Ding,[a] Hu Wu,[a] Fan Yang,[c] Chuanbo Gao,*[b] Yadong Yin[c] and Shujiang Ding*[a]*

[a] Department of Chemistry, School of Science, State Key Laboratory of Electrical Insulation and Power Equipment, Xi'an Key Laboratory of Sustainable Energy Material Chemistry, Xi'an Jiaotong University, Xi'an 710049, China. Emails: davidding1@mail.xjtu.edu.cn (D.D.); dingsj@mail.xjtu.edu.cn (S.D.)

[b] Center for Materials Chemistry, Frontier Institute of Science and Technology, State Key Laboratory of Multiphase Flow in Power Engineering, Xi'an Jiaotong University, Xi'an 710054, China. Email: gaochuanbo@mail.xjtu.edu.cn (C.G.)

[c] Department of Chemistry, University of California, Riverside, California 92521, United States

Supplementary Figures

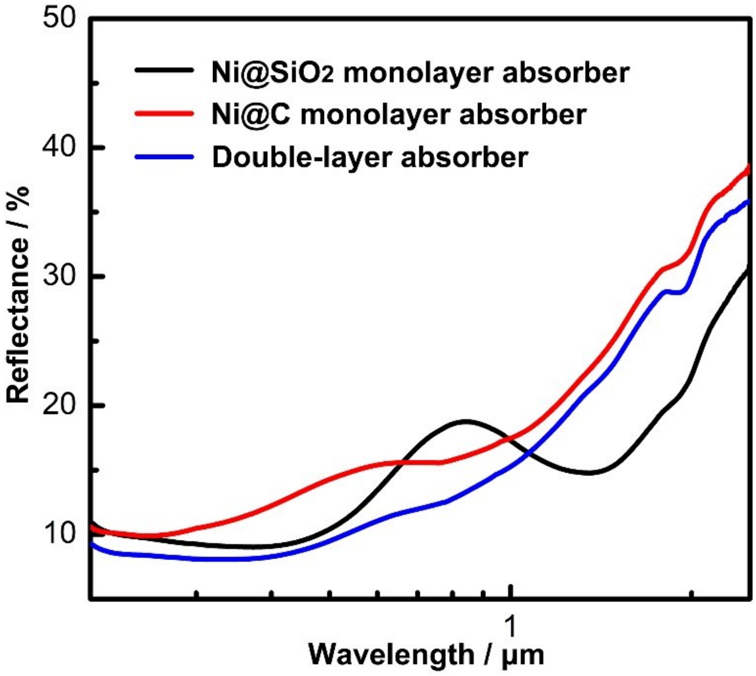

Fig. S1 UV-Vis-Near infrared (IR) diffuse reflectance of two types of selective absorbing film with the same thickness. Mono-layer solar absorber composed of only Ni@SiO_2 or Ni@C; Double-layer solar absorber composed of Ni@SiO_2 (top layer) and Ni@C (bottom layer), the substrate is stainless steel mesh. The application of two grade-layered absorbing films improves absorption in the UV-Vis-Near IR region and absorption selectivity.

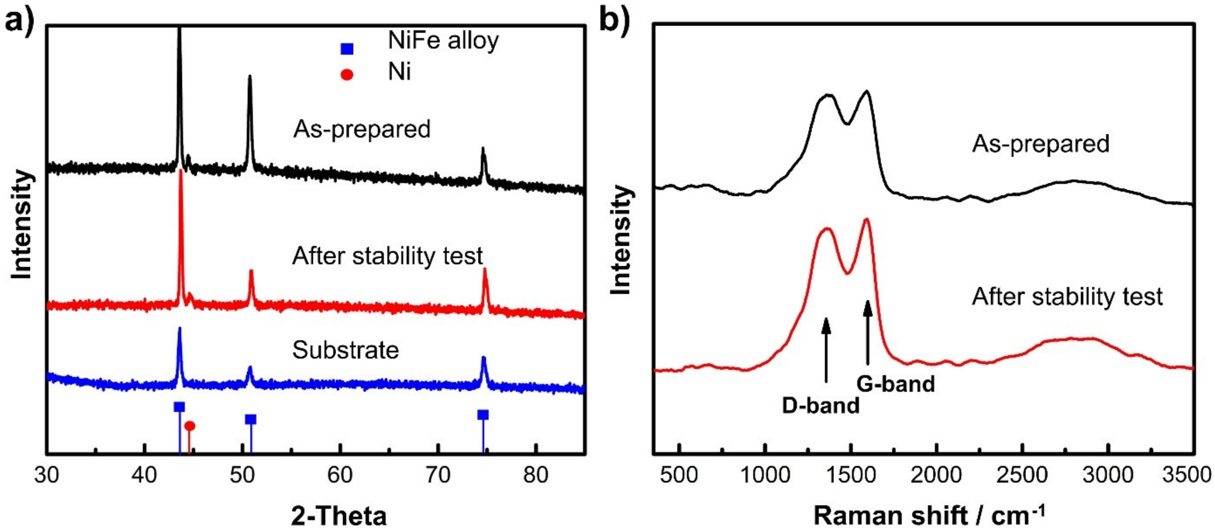

Fig. S2 XRD pattern (a) and Raman spectra (b) of SSA-Ni sample before and after stability test in water.

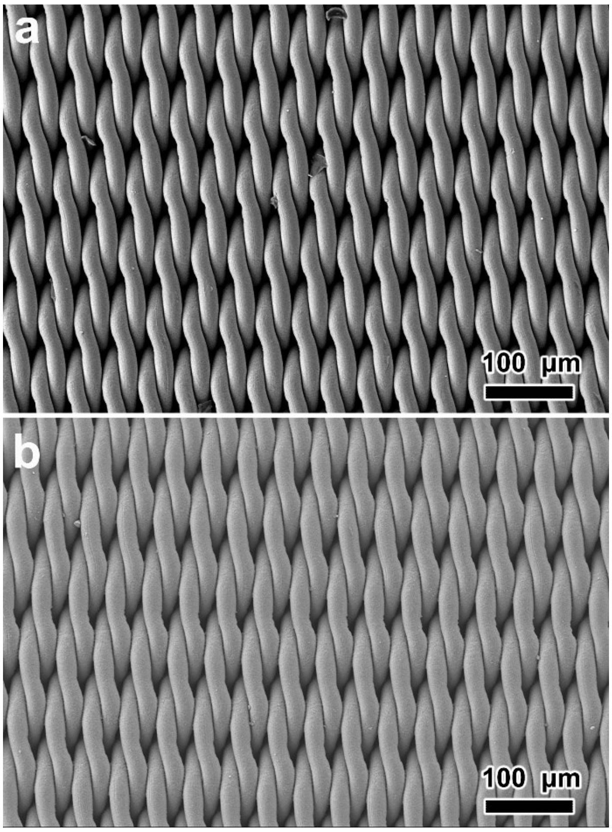

Fig. S3 SEM images of stainless steel mesh before (a) and after (b) deposited with graded absorbing layers of Ni@SiO_2 and Ni@C NPs.

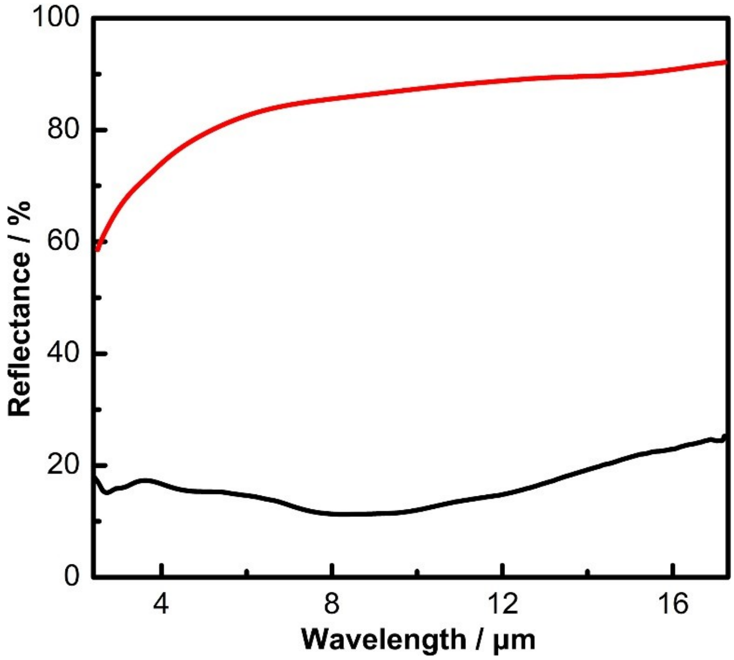

Fig. S4 Near-to-Middle IR diffuse reflectance of the SSA-Ni film (red line) and rGO-ag (black line). The SSA-Ni film shows sharp increase of reflectance from Near to Middle IR and keeps a high level in the entire middle IR region, whist rGO-ag exhibits low reflectance in the middle IR region similar to the optical property of blackbody.

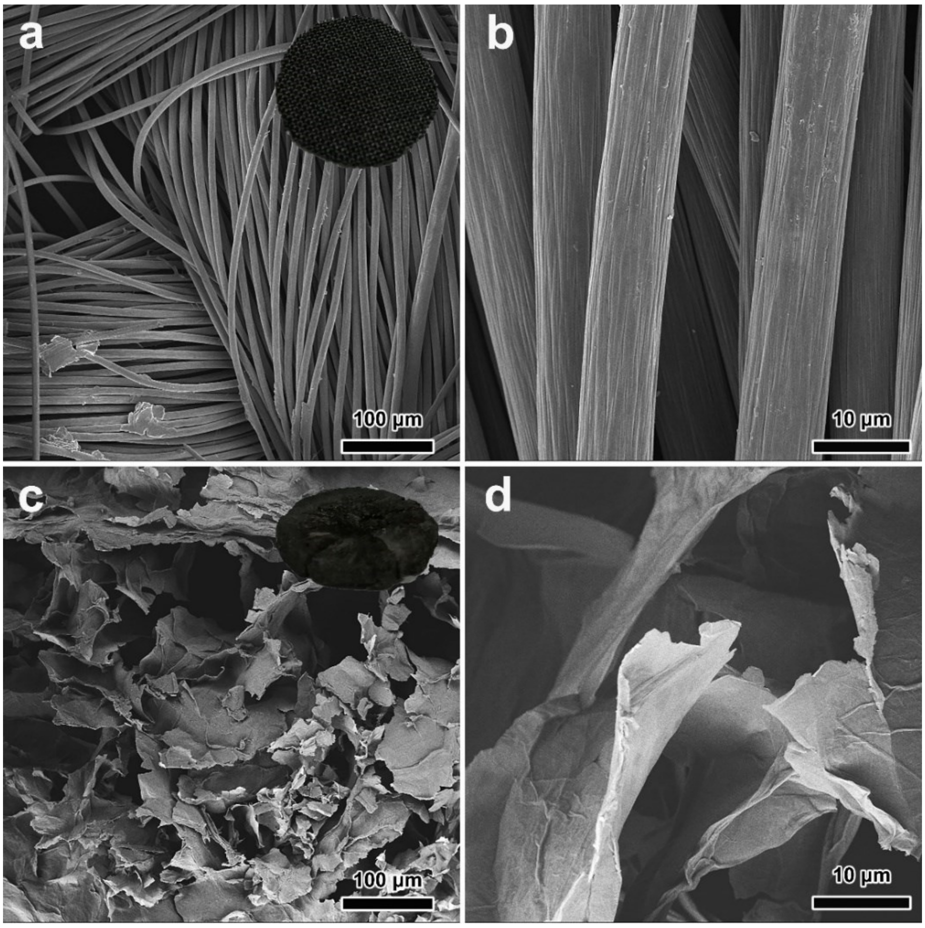

Fig. S5 SEM images of commercially available carbon fiber cloth (CF) (a, b) and prepared rGO-ag (c, d). Inserts are the sample photographs (CF, thickness: ~ 0.3 mm; rGO-ag, thickness: ~ 3 mm).

S1.1 Evaluation of thermal radiative loss

According to Kirchoff's law, spectral absorptance α (λ,θ) can be calculated directly by subtracting total reflectance ρ(λ,θ) for opaque materials,

$$\alpha\ (\lambda,\theta) = 1 - \rho\ (\lambda,\theta) \tag{1}$$

and

$$\varepsilon\ (\lambda,T) = \alpha\ (\lambda,T) \tag{2}$$

where ε (λ,T) is the spectral emittance, λ is the wavelength, θ is the incidence angle of light, and T is the given temperature. Thermal radiation is calculated from reflectance data fitted to blackbody curves

$$E(T) = \int_{\lambda_{min} = 0}^{\lambda_{max} = \infty} [1 - \rho(\lambda,T)]B(\lambda,T)d\lambda \tag{3}$$

and emittance is calculated from
$$\varepsilon(T) = \frac{E(T)}{\sigma T^4} \tag{4}$$

where σ is the Stefan-Boltzmann constant and B(λ,T) is the spectral irradiance of a blackbody curve from

$$B(\lambda,T) = \frac{c_1}{\lambda^5\left[e^{\left(\frac{c_2}{\lambda T}\right)} - 1\right]} \tag{5}$$

where c_1 and c_2 are Planck's first and second radiation constants, with values of 3.7405×10^8 $W\cdot\mu m^4\cdot m^{-2}$ and 1.43879×10^4 $\mu m\cdot K$, respectively.

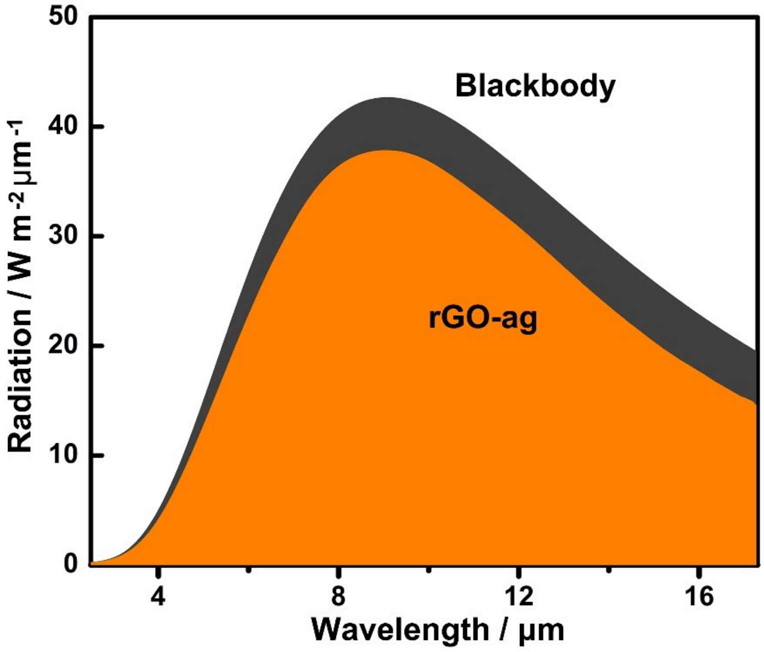

Fig. S6 The spectrally thermal radiative losses of rGO-ag *vs* blackbody at 46 ºC.

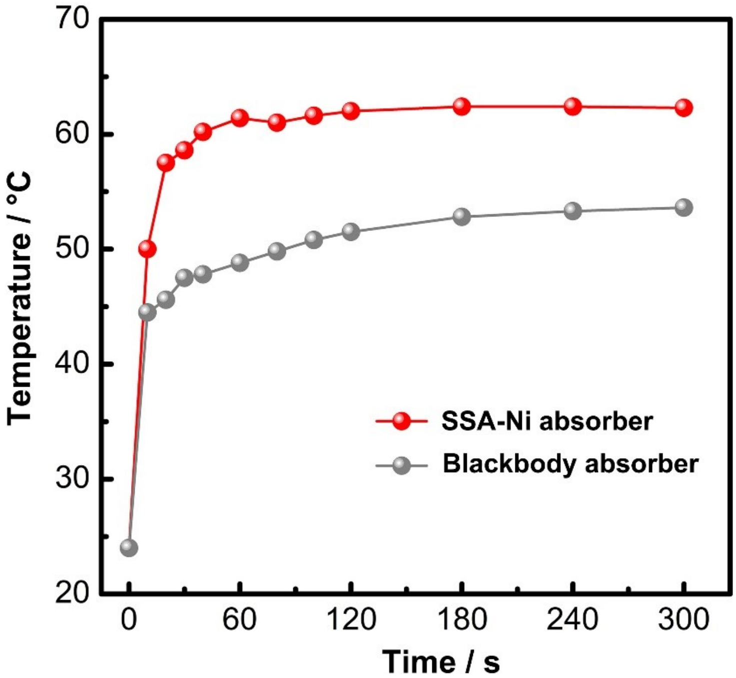

Figure S7. Temperature changes over time with different absorbers under 1 sun illumination.

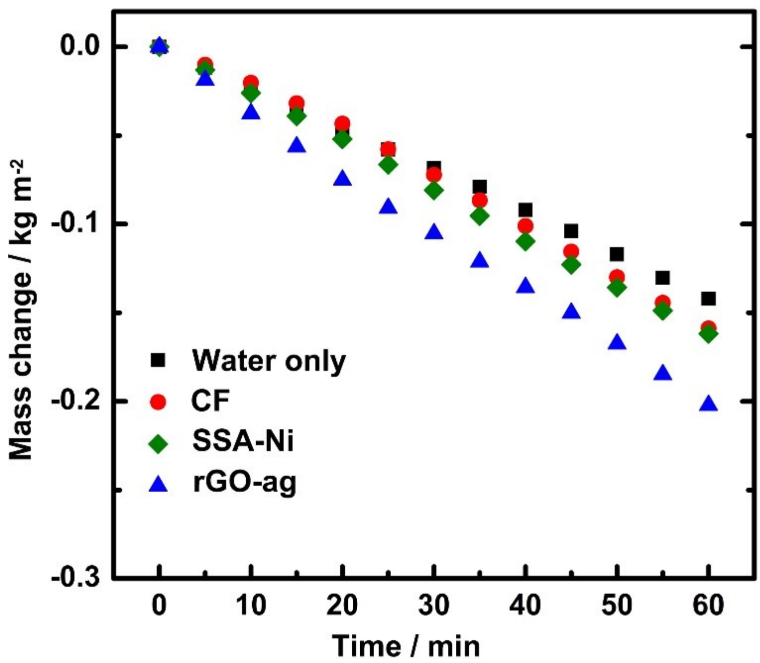

Fig. S8 Mass change of the water in different evaporation systems including water only, CF, SSA-Ni film, and rGO-ag under dark environment.

S1.2 Heat loss analysis

For the floating solar steam generator in our experiment, the heat loss mainly involves radiative and convective heat loss to the ambient and conductive heat loss to the underlying water, which can be expressed as

$$Q_{total} = A\varepsilon\sigma\left({T_1}^4 - {T_2}^4\right) + Ah\left(T_1 - T_2\right) + Cm\Delta T$$

Where Q_{total} is the total heat loss, A the surface area of the absorber (3.14 cm^2), ε the emittance of the absorbing surface (0.096), σ the Stefan–Boltzmann constant, $\boldsymbol{h}$ the convection heat transfer coefficient, $\boldsymbol{T_1}$ the average surface temperature of the absorbing surface (46 °C), $\boldsymbol{T_2}$ the ambient temperature (22 °C) in our experiment, $\boldsymbol{C}$ the specific heat capacity of water (4.2 J g^{-1} $°C^{-1}$), $\boldsymbol{m}$ the water weights, $\Delta\boldsymbol{T}$ the increased water temperature in 1 h. The radiative heat loss of the device can be calculated and accounts for ~1.5% of incoming solar energy; In calculation of convection heat loss, taking a natural convection heat transfer coefficient of 2.5 $W \cdot m^{-2} \cdot K^{-1}$, according to reference, the calculated convection heat loss accounts for ~ 6% of all incoming solar energy; The temperature of the water (m = 8.16 g) increased by ~ 1.2 °C during the whole experiment, therefore, the conduction heat loss can be calculated and accounts for ~ 3.6% of all the energy.

Table S1 Performance comparison of different water evaporation systems with solar absorbers of high solar absorption under 1sun.

Materials	**Evaporation rate ($kg\ m^{-2}\ h^{-1}$)**	**Evaporation rate Water only ($kg\ m^{-2}\ h^{-1}$)**	**Efficiency (%)**
Plasmonic absorber [1]	0.6	0.3	48
Graphite /carbon foam [2]	1.20	0.45	64
Black Al-Ti-O hybrid [3]	1.03	0.509	64.5
Wood/CNTs [4]	0.95	0.50	65
Black eggshell [5]	1.31	0.52	78
rGO aerogels-CNT-SA [6]	1.622	0.50	83
MXene Ti_3C_2 [7]	1.33	0.48	84
This work	1.52	0.31	91

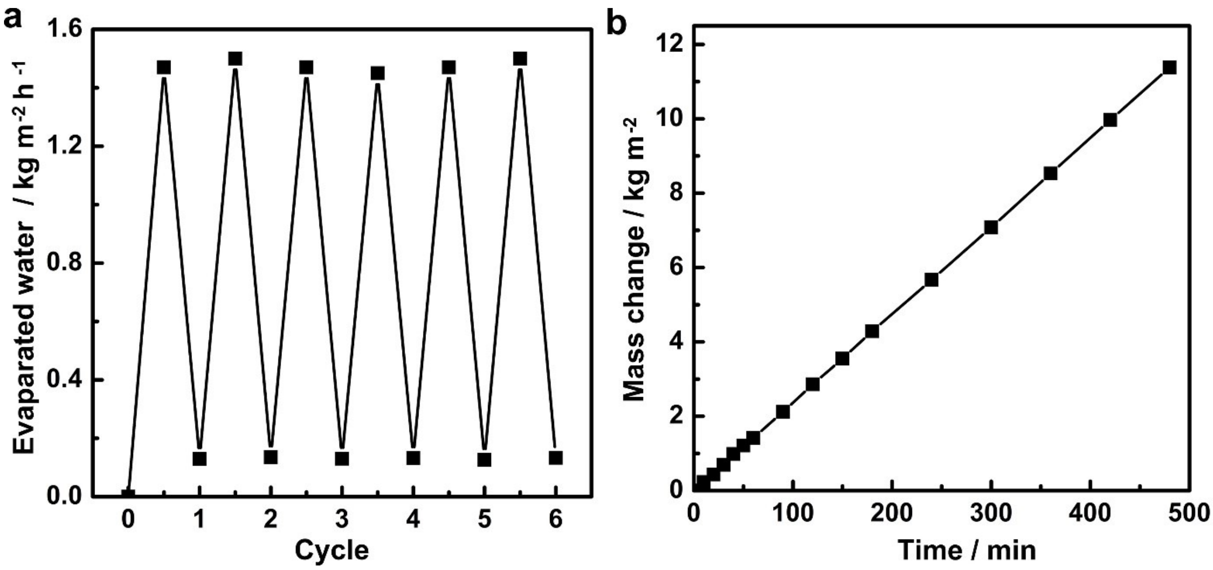

Fig. S9 Cycling performance (a) and continuous steam generation performance (b) of SSA-Ni evaporation system in simulated seawater of world sea.

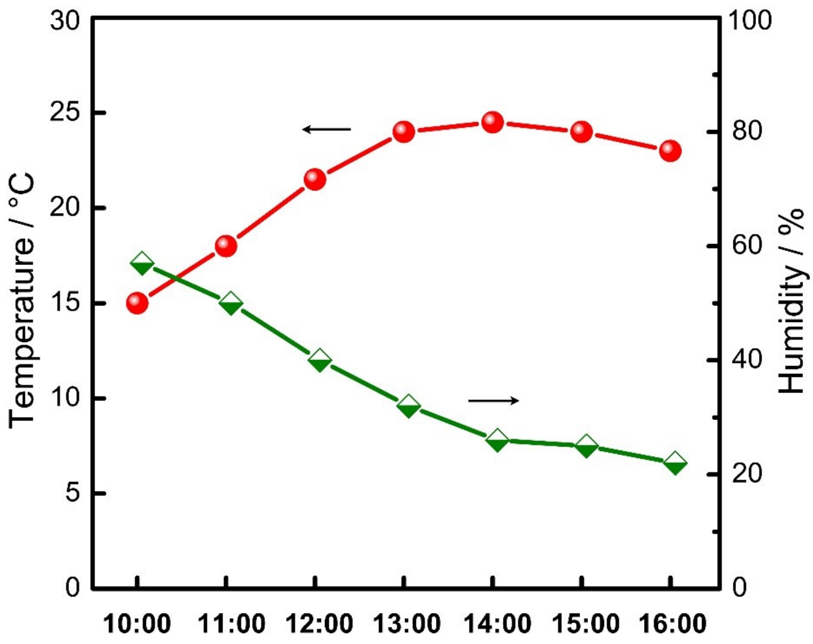

Fig. S10 The ambient temperature and humidity changes during 8 hours of outdoor solar desalination. Note: The data were collect on the roof of Hongrun Building at Innovation Harbor, Xi’an Jiaotong University (Xi’an, Shaanxi, China) on November 7, 2020.

References

(1) Zhou, L.; Zhuang, S.; He, C.; Tan, Y.; Wang, Z.; Zhu, J., Nano Energy 2017, **32**, 195-200.

(2) Ghasemi, H.; Ni, G.; Marconnet, A. M.; Loomis, J.; Yerci, S.; Miljkovic, N.; Chen, G., Nat. Commun. 2014, **5**, 4449.

(3) Yi, L.; Ci, S.; Luo, S.; Shao, P.; Hou, Y.; Wen, Z., Nano Energy 2017, **41**, 600-608.

(4) Chen, C.; Li, Y.; Song, J.; Yang, Z.; Kuang, Y.; Hitz, E.; Jia, C.; Gong, A.; Jiang, F.; Zhu, J. Y.; Yang, B.; Xie, J.; Hu, L., Adv. Mater., 2017, **29**, 1701756.

(5) Han, X.; Wang, W.; Zuo, K.; Chen, L.; Yuan, L.; Liang, J.; Li, Q.; Ajayan, P. M.; Zhao, Y.; Lou, J., Nano Energy 2019, **60**, 567-575.

(6) Hu, X.; Xu, W.; Zhou, L.; Tan, Y.; Wang, Y.; Zhu, S.; Zhu, J., Adv. Mater. 2017, **29**, 1604031.

(7) Li, R.; Zhang, L.; Shi, L.; Wang, P., ACS Nano 2017, **11**, 3752-3759.